No. 105 WAVELENGTH DEPENDENCE OF POLARZIATION. IX. INTERSTELLAR PARTICLES*

by THOMAS GEHRELS

February 27, 1967

ABSTRACT

Comparison of the wavelength dependence of interstellar polarization with that observed in reflection nebulae appears to rule out metallic and purely graphitic grains for the general interstellar medium. The observations on reflection nebulae are best explained with composite grains that have an absorptive nucleus of diameter 0.05 μ and an icy shell of diameter 0.3 μ. The visual albedo of the grains is near 0.5 and the asymmetry factor 0.6. Because of this asymmetry, reflection nebulae generally are not observable if the star is in front of the nebula. NGC 7023 has 4×10^{-10} grains/cm^3 and the visual optical depth within the nebula is only 0.2.

1. Introduction

MARTEL (1958) made extensive observations of the polarization of reflection nebulae, and she has given a detailed bibliography. Vanýsek and Svatoš (1964) and Roark (1966) have added new photometric studies. Elvius and Hall (1966) reported polarimetric as well as photometric observations. They found the amount of polarization in three reflection nebulae to increase, linearly and fairly steeply, with increasing wavelength. Their conclusion is used in this paper in a combination with the generally observed wavelength dependence of interstellar polarization.

Section II describes the observational results, including those of Elvius and Hall. The Mie calculations of Herman and Browning are described in Sec. III, and they are compared with the observations in Sec. IV. The Mie theory is for spherical particles, but recent experiments (Powell *et al.* 1966) indicate that the optical character of polydisperse, randomly aligned particles is not a sensitive function of particle shape. Most of the calculations in this paper are for single sizes, but a test case of size distributions is in Sec. V. The variation of the refractive index with wavelength has not been taken into account; the effect does not appear large enough to affect the conclusions of this paper. NGC 7023 is considered in Secs. VI and VII with the assumption of a uniform spherical reflection nebula with HD 200775 at its center, and an approximate knowledge ($\pm 20\%$) of the distance is needed. The optical depth within NGC 7023 is found from the scattering efficiency of the grains and from the observed brightness ratio of nebula and illuminating star; the interstellar extinction is thereby taken into account. In Sec. VIII we return to the interstellar grains in general, with a discussion of grain parameters and radiation pressure. This paper is primarily a reconnaissance of observational requirements and of techniques of interpretation, to be followed by improved work on reflection nebulae and interstellar polarization.

TABLE I. Particle diameters μ obtained from fitting the theory to observations of interstellar polarization and reddening.

Refractive index m	Diameter $2a$, from interstellar polarization	reddening
1.25	0.49	0.70
1.25–0.10i	0.31	...
1.50	0.28	0.35
1.50–0.10i	0.20	0.32
1.50–0.25i	0.16	...
1.41–1.41i	0.05	0.07

* Reprinted from the *Ast. J.*, Vol. 72, No. 5, June, 1967, with permission.

2. Observations

Table I reproduces the result of Paper II (Gehrels 1960a) in this series. The wavelength dependence of the interstellar polarization was compared with calculations by Mrs. E. v. P. Smith for perpendicular incidence on long cylinders; the resulting particle diameters are in Table I. The work on the interstellar polarization since then (for instance, see Coyne and Gehrels 1966) has confirmed these conclusions; there are differences from star to star but the general conclusion is well summarized in Table I. The observations on the wavelength dependence on reflection nebulae have been reported (Gehrels 1960b; also see Greenberg 1967), but the detailed comparison with the Mie theory is in this paper.

TABLE II. Observations in NGC 7023.

Object	Date UT Aug. 1959	$1/\lambda$	P (%)	θ (deg)
E-38″	1	1.82	8.5±0.9	150
		2.78	4.0	143
NE-38″	8	1.20	20.5	130
	2, 7	1.82	16.0	134
	2, 7	2.78	10.1	123
N-38″	6, 8	1.20	21.6	86
	3, 4	1.82	19.2	87
	3, 4	2.78	13.6	91
Central star	2	1.82	0.92±0.07	89
		2.78	0.85	84

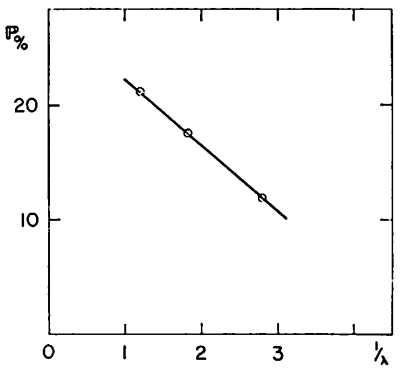

FIG. 1. Percentage polarization of the average of two regions in NGC 7023 as a function of the reciprocal of the wavelength (in microns).

Table II gives a few measurements in reflection nebula NGC 7023 [central star HD 200775, BD +67°1283, $\alpha(1959)=21^h01^m.4$, $\delta(1959)=68°00'$] made with the McDonald 82 in. in August 1959. The three filters are ultraviolet, green, and red, U', G', and R' of Table I of Gehrels and Teska (1960). The integration times are of the order of 1 min. The diaphragm is 22".58 in diameter. The regions are all at 38" (±2" p.e.) from HD 200775 in directions east, northeast, and north. At 38" from the central star NGC 7023 probably does not show emission, other than the reflected emissions of HD 200775 (Greenstein and Aller 1947, p. 142). The skies are measured at about 2'.6 due east or west of the central star. At this distance the sky settings are not entirely out of the nebula but the readings presumably are close to those of sky without stars; because of some obscuration, the spots could be chosen to be free of background stars.

The choice at the telescope is difficult to make. Because of nebular background, one overcorrects if the spot for the sky-background readings is chosen too close; however, because of background stars penetrating the dark nebula, one also overcorrects if the spot is too far.

The work on reflection nebulae and sky is time consuming, and measurements of various nights (6 and 8 August, for instance) are combined.

The directions of the position angles of the northeast and north regions (Table II) are perpendicular to the direction of HD 200775. It is therefore probable that this is the illuminating star, and that the material of the nebula is not appreciably aligned. The east region appears to be anomalous in percentage polarization and it is not further discussed in this paper.

Elvius and Hall (1966) observed colors and polarization of several spots in NGC 7023, as well as in the Merope Nebula and in NGC 2068. They used the Perkins telescope, in 1962–64, with focal-plane diaphragms of 29" and 42". The filter system is approximately that of U, B, and V. There is only one region of NGC 7023 in common with "northeast" in Table II, and Elvius and Hall found amounts of polarization that are about 0.7 times the amounts in Table II. The discrepancy is partially understood in terms of the corrections for sky light: it makes a large difference in the amount of light if the skies are measured farther out than the above-mentioned 2'.6. Corrections for scattered light from the central star also are a problem. For the measurements of Table II, the 82-in. mirror was washed (thanks to Mr. Marlyn Krebs), and special baffling inside the photometer was installed; approximate checks of the absence of scattered light were made, but not in great detail and it is possible that a small effect was overlooked.

The remarkable conclusion of Elvius and Hall is that the wavelength dependence of most regions in NGC 7023, the Merope Nebula, and NGC 2068 is approximately the same. I also found this in some (unpublished) measurements on NGC 2068.

Figure 1 shows the average of the polarizations for "north" and "northeast" in Table II. The observations of Elvius and Hall give approximately the same wavelength dependence for several spots in three reflection nebulae; the effect of their smaller amount, observed northeast of HD 200775, is discussed in Sec. V. In any case, some smoothing over regional differences and observational errors is included by taking the average of two regions, and the fitting of the Mie theory will, therefore, be made to the line in Fig. 1.

3. *Mie Calculations*

For the interpretations below, the tables of LaMer (1943) are used. In addition, especially for absorbing particles, new calculations were made with the IBM 7072 of the Numerical Analysis Laboratory at the University of Arizona. The Mie program is that of Dr. B. M. Herman and Maj. Genl. (ret.) S. R. Browning, to whom I am greatly indebted. Details of the Mie calculations have been published (viz., Herman and Battan 1963).

Table III gives an approximate identification of refractive indices, most of which were taken from van de Hulst (1957, Table 26).

Figures 2 and 3 show a sample of the present calculations. The format is that of van de Hulst (1957, pp. 152–153), who gives plots for spheres with refractive index $m=1.33$, 1.50, 1.55, and 2, and for

TABLE III. Identification of refractive indices, for aerosols at wavelength 0.5 μ.

Substance	Refr. index
Ices	1.3
Impure ices	$1.3-0.05i$
Glasses	1.5
Impure glasses	$1.5-0.05i$
Carbon	$1.6-0.7i$
Metallic, generally	$1.4-1.4i$
Nickel and zinc	$1.5-3i$
Copper	$1.1-2i$
Sodium	$0.06-2i$

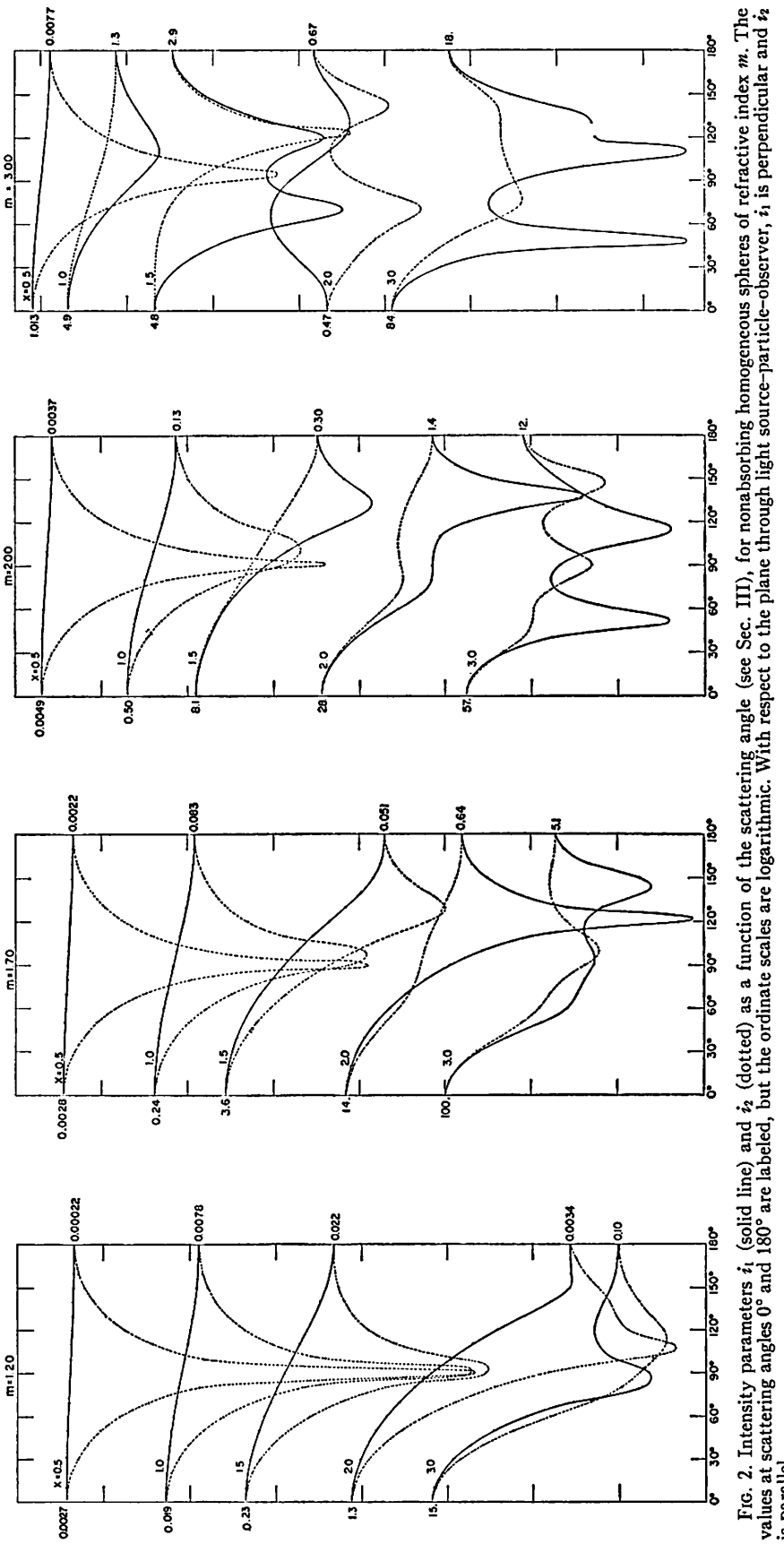

FIG. 2. Intensity parameters i_1 (solid line) and i_2 (dotted) as a function of the scattering angle (see Sec. III), for nonabsorbing homogeneous spheres of refractive index m. The values at scattering angles 0° and 180° are labeled, but the ordinate scales are logarithmic. With respect to the plane through light source–particle–observer, i_1 is perpendicular and i_2 is parallel.

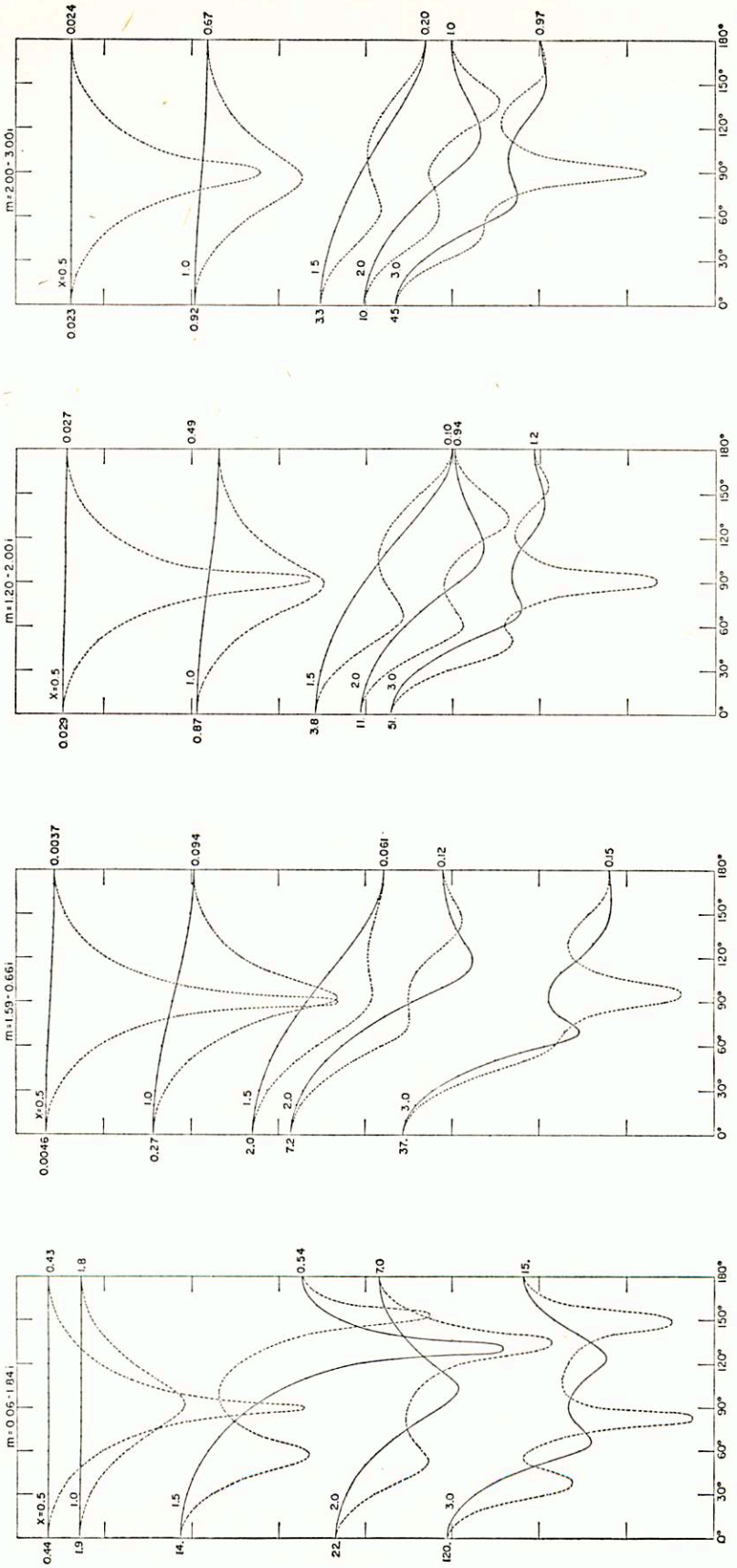

FIG. 3. As in Fig. 1, but for absorbing homogeneous spheres.

TABLE IV. Computed polarizations and particle diameters μ for star *at the center* of nebula; scattering angles 20–160°.

Refr. index	$2\pi a/\lambda$	P%	Particle diameter at $1/\lambda=$ 1.20	1.82	2.78
	1.5	+36.9			
1.20	2.0	+25.4	0.59	0.43	0.33
	3.0	+11.4			
	1.8	+25.2			
1.33	2.0	+18.3	.50	.35	.25
	2.5	+10.0			
	1.5	+31.9			
1.44	1.8	+18.6	.47	.31	.22
	2.0	+11.2			
	1.5	+27.6			
1.55	1.8	+10.5	.42	.29	.20
	2.0	− 0.9			
	1.0	+40.1			
1.70	1.5	+18.2	.38	.26	.19
	2.0	− 1.9			
	1.5	+34.1			
1.33–0.15i	2.0	+20.2	.51	.38	.31
	3.0	+ 9.8			
	1.5	+33.5			
1.33–0.30i	2.0	+21.2	.53	.41	.36
	3.0	+12.8			
	1.5	+32.7			
1.33–0.60i	2.0	+23.2	.61	.59	...
	3.0	+18.7			
	1.0	+40.5			
1.57–0.15i	1.5	+27.1	.44	.31	.22
	2.0	+ 9.1			
	1.0	+40.4			
1.57–0.30i	1.5	+27.5	.46	.32	0.23
	2.0	+12.0			
	1.0	+40.0			
1.59–0.66i	1.5	+27.3	0.48	0.34	...
	2.0	+16.7			
	1.5	+18.1			
0.06–1.84i	2.0	+31.7	...	...	...
	3.0	+32.9			

cylinders with $m=1.50$. The parameter $x=2\pi a/\lambda$, where a is the particle radius and λ is the wavelength of the light. In this paper the *scattering angle* is used, which is the supplement of the phase angle (used in the tables of LaMer). For nonpolarized incident light of unit intensity, the intensity (in erg cm^{-2} sec^{-1}, for instance) of a single particle observed at distance r is (van de Hulst 1957, p. 129)

$$(I_1+I_2)=(i_1+i_2)\lambda^2/8\pi^2r^2, \qquad (1)$$

where I_1 and I_2 are the scattered intensities in two orthogonal directions and i_1 and i_2 are the computed and plotted quantities. I am indebted to Mrs. Tricia Coffeen for plotting Figs. 2 and 3. We also have graphs for $m=1.70$–$4.00i$ and $m=3.00$–$4.50i$, which are almost identical to those of $m=2.00$–$3.00i$; graphs for $m=0.56$–$3.01i$ are also quite similar.

Figure 4 shows a cross section of an idealized spherical nebula with the illuminating star at its center. The discussions of this paper are for uniform space density of the particles in NGC 7023.

In Tables IV–X the weighted mean polarizations are calculated from the values of i_1 and i_2 over a range of scattering angles. The weights depend: on R^{-2}, where R is the distance from the illuminating star; on V, which is the volume of the segment that has, on the average, a certain scattering angle; and on the scattering efficiency of each particle into a given direction. Conveniently,

$$R^{-2}\times V\cong\text{const} \qquad (2)$$

(demonstrated in Table XII of Sec. VI), so that the weighting is only with (i_1+i_2). From i_1 and i_2, tabulated at 10° intervals in the Herman and Browning program, one calculates

$$P=100(\Sigma i_1-\Sigma i_2)/(\Sigma i_1+\Sigma i_2), \qquad (3)$$

where the summations in Table IV, for instance, are over the 20–160° range. A plus sign for P in Tables IV–IX indicates that the electric vector maximum is perpendicular to the direction of the illuminating star (as is generally observed in NGC 7023; see Sec. II); a minus sign is for radial direction.

4. *Interpretations*

In Table IV the illuminating star is at the center of a uniform spherical nebula. At the values of refractive index m and of $x=2\pi a/\lambda$, the percentage polarization P is calculated (Sec. III). The computed P values are plotted as a function of x and the observed polarizations of Fig. 1 (21.1% at $1/\lambda=1.20$, 17.6% at 1.82, and 11.9% polarization at $1/\lambda=2.78$) are then used to find the values of $2a$. For none of the refractive indices in Table IV is $2a$ constant; in other words, the observed wavelength dependence of polarization is not reproduced by the calculations.

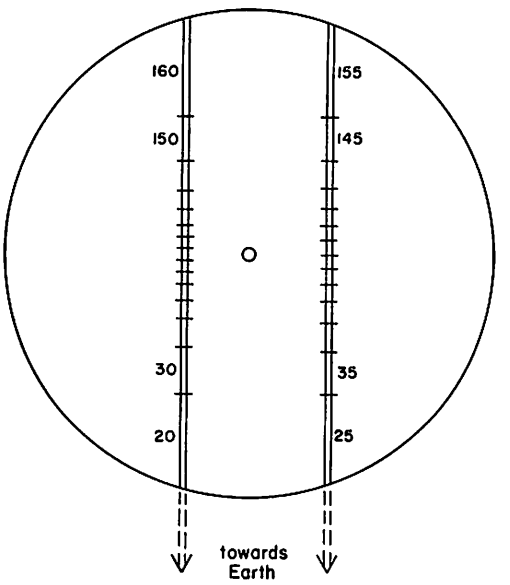

FIG. 4. Cross section through a spherical reflection nebula that has the illuminating star at its center. Volume segments are labeled with their mean scattering angle. *On the left*, for Secs. IV and V; *on the right*, for Sec. VI.

TABLE V. Computed polarizations for star *in front* of nebula; scattering angles 120–160°.

Refr. index	$2\pi a/\lambda$	$P\%$
	1.2	+32.5
	1.5	+41.0
	1.8	+70.8
1.33	2.0	+ 8.3
	2.4	− 4.1
	2.5	+ 2.1
	3.0	+50.8
	3.6	−31.0
	1.2	+34.6
	1.5	+47.9
	1.8	+50.8
1.44	2.0	−33.2
	2.4	−14.8
	2.5	− 7.7
	3.0	−16.0
	3.6	−39.1
	1.0	+30.3
1.33–0.15*i*	1.5	+42.7
	2.0	−30.6
	3.0	+81.0
	1.0	+30.3
1.33–0.30*i*	1.5	+38.5
	2.0	−31.3
	3.0	+28.5
	1.0	+29.6
1.33–0.60*i*	1.5	+24.0
	2.0	− 9.9
	3.0	− 0.4
	1.0	+32.6
1.57–0.15*i*	1.5	+65.5
	2.0	−53.4
	3.0	−48.0
	1.0	+32.6
1.57–0.30*i*	1.5	+49.5
	2.0	−46.9
	3.0	−43.5
	1.0	+31.4
1.59–0.66*i*	1.5	+41.9
	2.0	−10.9
	3.0	−25.0

In Table V the illuminating star is placed in front of the nebula. The computed wavelength dependence now is even steeper than that in Table IV. The abrupt change from positive to negative polarization can be seen in Figs. 2 and 3. The computed wavelength dependence is very irregular near scattering angle 140°. The filters used for the observations in NGC 7023 are narrow enough so that such strong variations from positive to negative polarization, and vice versa, would have been detected. It is possible that a very wide dispersion of diameters and refractive indices would average out the steep variations; but the computed wavelength dependence of polarization would still be much too steep in the neighborhood of $x=1.5$. In any case, very wide dispersions are unlikely since they would "wash out" the marked shape of Fig. 1 and of the interstellar polarization dispersion.

In Table VI the illuminating star is behind the nebula. The three columns of $2a$ now generally are similar; the observed wavelength dependence is reproduced by the Mie calculations. Next, a comparison is made, for various refractive indices, with the results of interstellar polarization and reddening (Table I). The best consistency appears for values of

$$2a \cong 0.3\ \mu \tag{4}$$

and

$$(1.2-\epsilon i) < m < (1.6-\epsilon i) \tag{5}$$

with

$$0.1 < \epsilon < 0.4. \tag{6}$$

The calculations for m without imaginary component in Table VI have not been carried out for refractive indices greater than 2.0 because the (approximate) linearity of P as a function of x breaks down. The wavelength dependence of polarization near $x=1.2$ would be much steeper than is observed.

Table VII supplements Tables IV and VI with modifications of the range of scattering angles. The strong forward scattering at 10°, which is relatively little polarized, tends to dilute the polarizations. It is seen that 10–50° is too extreme; at no value of x do the calculations give the high observed polarizations (20%). To the contrary, the range 30–80° gives the wavelength dependence too steep. A range slightly different from 20–60° (for instance 10–70°) is acceptable, and the interpretations made with Table VI appear unchanged.

TABLE VI. Computed polarizations and particle diameters μ for star *behind* nebula; scattering angles 20–60°.

Refr. index	$2\pi a/\lambda$	$P\%$	Particle diameter at $1/\lambda=$ 1.20	1.82	2.78
	1.5	+22.0			
1.20	2.0	17.7	0.42	0.36	0.32
	3.0	10.5			
	1.5	19.9			
1.33	2.0	13.8	.36	.29	.25
	3.0	3.9			
	1.0	23.6			
1.44	1.5	17.7	.32	.26	.22
	2.0	10.5			
	1.0	22.9			
1.55	1.5	14.9	.30	.23	.19
	1.8	9.0			
	0.5	25.7			
	1.0	21.9			
1.70	1.5	10.1	.26	.21	.17
	2.0	7.2			
	0.5	25.6			
2.00	1.0	19.0	.22	.17	.14
	1.5	1.1			
	1.5	20.0			
1.33–0.15*i*	2.0	16.0	.36	.32	.30
	3.0	8.9			
	1.5	20.5			
1.33–0.30*i*	2.0	17.8	.37	.35	.35
	3.0	12.1			
	1.5	22.2			
1.33–0.60*i*	2.0	21.2	.53	.54	.55
	3.0	17.9			
	1.0	22.6			
1.57–0.15*i*	1.5	15.2	.29	.24	.21
	2.0	11.0			
	1.0	22.6			
1.57–0.30*i*	1.5	16.4	.29	.25	.23
	2.0	13.2			
	1.5	19.1			
1.59–0.66*i*	2.0	17.7	0.26	0.34	0.39
	3.0	+13.7			

TABLE VII. Computed polarizations and particle diameters μ for various ranges of the scattering angle.

Scattering angles	Refractive index	$2\pi a/\lambda$	P%	Particle diameter at $1/\lambda$= 1.20	1.82	2.78
		1.8	+20.0			
	1.33	2.0	14.3	0.47	0.33	0.24
		2.5	7.5			
10–160°		1.5	26.4			
	1.44	1.8	14.8	.44	.31	.22
		2.0	8.8			
		0.5	15.9			
	1.33-0.15i	1.0	14.5	···	···	.18
		1.5	12.1			
		0.5	15.9			
10– 50	1.33-0.30i	1.0	14.6	···	.06	.18
		1.5	12.4			
		0.5	15.8			
	1.33	1.0	14.6	···	···	.17
		1.5	12.1			
		1.5	34.2			
30– 80	1.33-0.15i	2.0	25.4	.60	.43	.34
		3.0	11.7			
		1.0	21.1			
	1.33-0.15i	1.5	15.6	.27	.24	.23
		2.0	12.1			
		1.0	19.2			
	1.33-0.30i	1.5	16.0	.17	.22	.26
		2.0	13.3			
10– 60		1.0	19.9			
	1.20	1.5	17.2	.21	.25	.26
		2.0	13.5			
		0.5	20.8			
	1.70	1.0	17.4	.13	.16	.15
		1.5	8.0			
		1.5	21.8			
	1.33-0.15i	2.0	14.8	.40	.32	.27
		3.0	5.7			
10– 80		1.5	22.0			
		2.0	16.1	0.41	0.33	0.29
	1.33-0.30i	3.0	+ 7.8			

The range of 10–80° appears less likely; the wavelength dependence again is becoming too steep.

The principal conclusion is that purely absorptive grains in the general interstellar medium are ruled out. Qualitatively one could already see in Fig. 3 the steep increase in polarization to occur, for scattering angles 20–60°, at $x \simeq 2$; in Fig. 1 it occurs at $1/\lambda \simeq 2.5$; it follows that $2a \simeq 0.25\,\mu$. The wavelength dependence of three reflection nebulae was found approximately the same. On the assumption that these three are typical interstellar clouds, one brings in the comparison with the "interstellar" results of Table I, and the above $0.25\,\mu$ for absorptive grains is then ruled out. Absorptive grains as condensation nuclei for the general interstellar particles are considered next.

Table VIII gives some calculations for concentric shells. The refractive indices and the diameters (in microns) are listed in the first column with subscripts c for the *c*ore and s for the *s*hell. The value of $1/\lambda$ (in reciprocal microns) for which the calculations are made is in the second column. The three cases of star/nebula geometry of Tables IV, V, and VI are in the next three columns: scattering angles 20–160°, 120–160°, and 20–60°, respectively.

The first model in Table VIII is a graphite grain with $0.08\,\mu$ diameter, having an ice coating to $0.224\,\mu$; this particle was suggested by Wickramasinghe (1963) as providing a fair fit to the observed interstellar reddening. Since the wavelength dependence of Fig. 1 is not quite reproduced, the outside diameter is enlarged (second model) and impurities are added to the ice (third model). The last model in Table VIII has a small metallic core and a shell of ice, as proposed by Whitney (1965) to explain the 4430 Å band. It is seen in Table VIII that the observations of Fig. 1 can indeed be reproduced with the coated grains of the proper outside dimension ($2a \cong 0.3\,\mu$). Straight averaging of $P(\lambda;$ 20–60°) of the first and last models reproduces Fig. 1 precisely.

The high imaginary component of expression (6), needed for the best fit to Fig. 1, is rather alarming. What type of material in interstellar space could yield homogeneous grains with such a refractive index? "Dirty ices" as proposed by Oort and van de Hulst (1946) have $m = 1.3\text{–}0.05i$ (in visual light). Here may be an argument in support of the composite grains (I am indebted to Dr. Greenberg for pointing this out).

5. *Size Distributions*

Table IX has computations of the percentage polarization for two size distributions, and also for a single size, of homogeneous grains with refractive index $1.40\text{–}0.21i$. The three computed columns are for scattering angles 20–160°, 120–160°, and 20–60°, respectively. The Oort–van de Hulst size distribution is used, for example in the first case: with relative weight, by number of particles, of 0.48 for particle diameter $0.16\,\mu$,

TABLE VIII. Computed polarizations for coated particles.

Grain specifications; *c*ore and *s*hell	For $1/\lambda$	Percentage polarization having star at center	in front	behind
$m_c = 1.63\text{–}0.82i$	0.91	+42.3	+27.9	+25.9
$m_s = 1.33$	1.11	+42.1	+28.5	+25.4
$2a_c = 0.08$; $2a_s = 0.224$	1.43	+41.4	+29.8	+24.4
	2.00	+37.3	+35.2	+21.3
	3.33	+14.3	+27.5	+11.8
$m_c = 1.63\text{–}0.82i$	0.91	+36.7	+37.7	+20.8
$m_s = 1.33$	1.11	+27.3	+60.4	+16.8
$2a_c = 0.08$; $2a_s = 0.50$	1.43	+12.8	− 8.3	+12.0
	2.00	+ 5.1	+35.3	+ 3.8
	3.33	− 1.2	+56.9	− 2.2
$m_c = 1.63\text{–}0.82i$	0.91	+35.9	+39.2	+20.7
$m_s = 1.33\text{–}0.13i$	1.11	+27.2	+65.2	+17.6
$2a_c = 0.08$; $2a_s = 0.50$	1.43	+15.5	− 6.6	+14.3
	2.00	+ 8.3	+29.6	+ 7.5
	3.33	+ 2.2	+49.6	+ 1.7
$m_c = 1.40\text{–}1.40i$	0.91	+43.7	+32.1	+23.2
$m_s = 1.33\text{–}0.13i$	1.11	+36.5	+38.1	+21.0
$2a_c = 0.02$; $2a_s = 0.40$	1.43	+25.6	+69.5	+17.2
	2.00	+12.5	+28.5	+12.3
	3.33	+ 4.5	+77.3	+ 3.2

TABLE IX. Computed polarizations for various size distributions.

Specifications $m=1.40-0.21i$	For $1/\lambda$	Percentage polarization having star at center	in front	behind
Distribution about $2a=0.32\,\mu$	0.80	+42.3	+30.6	+27.3
	1.20	33.5	+34.1	19.6
	1.85	20.6	+33.8	14.6
	2.78	11.8	+28.6	9.6
Distribution about $2a=0.16\,\mu$	0.80	42.4	+27.6	26.1
	1.20	42.0	+28.8	25.1
	1.85	39.2	+32.1	22.4
	2.78	26.7	+33.0	18.1
No size-distr.; $2a=0.32\,\mu$	0.80	41.9	+29.1	24.9
	1.20	38.8	+34.6	21.9
	1.85	21.1	− 9.0	16.0
	2.78	+10.0	+82.7	+ 9.3

0.30 for 0.24 μ, 0.15 for 0.32 μ, 0.05 for 0.40 μ, and 0.02 for 0.48 μ. The second case has the same distribution but all particle diameters are smaller by a factor 2. This case, incidentally, gives less polarization dispersion than that of Fig. 1. The last case is for the single size of diameter 0.32 μ.

It is seen from the comparison in Table IX that the conclusions in the previous section, made for an "infinitely narrow" size distribution, are practically unchanged when an Oort–van de Hulst distribution, centered on the same particle size, is considered. This should not be surprising as Oort and van de Hulst (1946, Fig. 9) have shown how steep their actual size distribution apparently becomes because of the greater scattering efficiency of the larger particles.

It is noted that while the Oort–van de Hulst distribution centers on $2a=0.6\,\mu$, the present calculations, and also those on the interstellar effects (Table I), are centered on half that size, $2a=0.3\,\mu$.

Table X shows a few of the fittings to the observations of Elvius and Hall (1966); the table has the same type of analysis as is in Tables IV–VII, but the computed polarizations are not listed again. The observations were taken from a manuscript kindly supplied by the authors at the time of the August 1965 conference (Greenberg 1967): at 4 mm N and 4 mm E, which is at 38″ from HD 200775, 12.6% polarization with a filter at 5740 Å, 9.5% at 4460 Å, and 7.4% at 3760 Å. By extrapolation and interpolation the following normal points were obtained, and used for Table X: 15.8% at $1/\lambda=1.20$, 12.1% at $1/\lambda=1.82$, and 6.7% at $1/\lambda=2.78$. It is seen that a fit can be made nearly at the same grain parameters as before, stated in expressions (4)–(6), but at slightly smaller scattering angles than before so that the star is farther behind the nebula.

6. *Space Density in NGC 7023*

A photometric distance determination of HD 200775 is made as follows. Mr. R. I. Mitchell (personal communication) obtained the values: $V=7.43$, $B-V=+0.38$, $U-B=-0.41$:, $V-R=+0.57$, and $R-I=+0.30$ mag. With these values, and reference to the papers by Johnson (1965) and Johnson and Borgman (1963), the ratios of Table XI are obtained. A precise determination of the ratio of total to selective absorption cannot be made without far-infrared photometry, but a value of 4.2 appears consistent also with the interpolation formula

$$A_V/E_{B-V}=(0.96+0.58E_{V-I}/E_{B-V})E_{V-I}/E_{B-V}, \quad (7)$$

given by Johnson and Borgman. The spectral type of HD 200775 has been given as B2p by Hubble (1922) and by Keenan (1936), dB3ne by Greenstein and Aller (1947), B3 by Mendoza (1958), and B5e by Stebbins, Huffer, and Whitford (1940). The ultraviolet excess ratio in Table XI appears more consistent for B2V than for B3V, and I therefore adopt, for the purpose of excess-to-absorption conversion, B2V. The absolute magnitude for B2V is given by Blaauw (1963) as −2.5. The color excess $E_{B-V}=0.62$ mag. The distance modulus $(V-M_V)=7.3$ mag, and the distance is 0.29 kpc, or

$$r=0.9(\pm 0.2\ \text{p.e.})\times 10^{21}\ \text{cm}. \quad (8)$$

This agrees with the distance of 0.3 kpc determined from proper motions by Lundmark (1922).

TABLE X. As for Tables IV–VII, but fitted to the observations of Elvius and Hall (1966).

Refractive index	Scattering angles	Particle diameter at $1/\lambda=$ 1.20	1.82	2.78
2.00	20– 60°	0.27	0.21	0.16
1.55	20– 60	.38	.28	.22
1.20	20– 60	.61	.49	.40
1.57–0.66i	20– 60	.66	.59	.54
1.33–0.15i	20–160	.63	.48	.37
	20– 60	.55	.45	.38
	10– 60	.42	.35	.30
	10– 50	.14	.26	.33
1.33–0.30i	20–160	.70	.54	.43
	20– 60	.62	.52	.45
	10– 60	.41	.39	.37
	10– 50	0.19	0.27	0.32

This agrees with the distance of 0.3 kpc determined from proper motions by Lundmark (1922).

Table XII gives the fluxes intercepted and scattered towards the earth by various groups of grains. At each scattering-angle interval, the values of $\langle i_1+i_2\rangle$ are obtained by straight averaging in the tables of LaMer (1943) for $m=1.33$ and 1.44 at $x=1.5$ and 1.8 (for $\lambda=0.56\,\mu$ and $2a=0.30\,\mu$), this result, for homogeneous particles, is in the second column. The third column is for coated particles and the averaging is in the Herman–Browning tables for mixture d (identified in Table XIII, below) at values of $1/\lambda=1.43$ and 2.00; this case, rather than that of the homogeneous particles, is pursued in the remaining columns of Table XII. The Distance and Volume columns are for the geometry of Fig. 4, based on the distance of HD 200775 of 0.29 kpc,

for one square second of arc observed at 0'.8 from the central star (in order to fit to Martel's observation; see below). The Flux per Particle (fifth column) is

$$F=\langle(i_1+i_2)\rangle\lambda^2/8\pi^2R^2, \quad (9)$$

where R is the distance of the particle from HD 200775 (fourth column). The nebular brightness is compared (below) with that observed on the star. The r^{-2} term in expression (1) is thereby taken into account—as well as the interstellar extinction—while the R^{-2} term normalizes the flux incident on the particle.

Incidentally, the last column of Table XII is nearly the same as the third, but for a constant factor, since the product of volume and inverse square distance is nearly a constant [expression (2)]. The essential weighting factor is $\langle i_1+i_2\rangle$; it shows the strong forward directivity of scattering by these grains. The range 20–70° contributes most to the observed light; addition of the 70–80° interval, for instance, would add only 6% to the light. The last column of Table XII also shows how hard, or impossible, it would be to observe a reflection nebula if the star were in front, rather than behind, the nebula: the sum over 110–160° is 330 compared to 8163 for 20–70°. For NGC 7023, one of the brightest reflection nebulae, the nebular brightness would be about one-tenth that of the sky. (Exceptionally high space densities might make the nebula observable.)

TABLE XI. Color-excess ratios, and ratio of total to selective absorption.

Object	$\frac{E_{U-V}}{E_{B-V}}$	$\frac{E_{V-R}}{E_{B-V}}$	$\frac{E_{V-I}}{E_{B-V}}$	$\frac{A_V}{E_{B-V}}$
Cepheus	1.84	0.85	1.60	6
II Per	1.68	0.81	1.69	3.75
Orion belt	1.82	1.13	2.26	4.8
HD 200775 B3V	1.52	1.09	1.97	4.2
HD 200775 B2V	1.73	1.08	1.92	

It is seen in Sec. IV (Tables VI and VII) that 20–60°, or perhaps 15–65°, is the most likely range of scattering angles for observations made at 38″ from HD 200775. In Table XII (at 0'.8 from HD 200775) such ranges correspond to 20–70°. The sum in the last column of Table XII therefore is taken over 20–70°; it is 8.2×10^3. Martel (1958) gives the brightness, after subtraction of sky brightness, per square second of arc: it is 21.3 (±0.2) visual magnitude at 0'.8 from HD 200775. This magnitude when compared to that of HD 200775 (7.43 mag; see above) gives a brightness ratio of 2.8×10^{-6}. It follows that there are 3.4×10^{-10} grains/cm³.

The precision of the derived density is of the order of ±40% (p.e.), determined by the uncertainty in the distance, the photometry, the composition of the particles, and the adopted range of scattering angles. Since $R^{-2}\times V\simeq$const, the uncertainty in the distance determination does not affect the polarimetry conclusions of Sec. IV, and it affects the density determination only in the first power, i.e., in the scale conversion of sec of arc to cm of NGC 7023. As for the particle composition, the homogeneous case of $m\simeq1.4$ (second column of Table XII) gives 4.0×10^{-10} grains/cm³ and the case of $m=1.4-0.3i$ (still $2a=0.30\,\mu$) gives 3.2×10^{-10} grains/cm³.

7. *Self-Extinction and Multiple Scattering*

The optical depth is given by

$$\tau=\pi a^2Q_{ext}NL, \quad (10)$$

where the particle radius $a=1.5\times10^{-5}$ cm; the efficiency factor for the total attenuation $Q_{ext}\simeq1.0$ (Table XIII, below) at $1/\lambda=1.82$; the particle density $N=3.8\times10^{-10}$ cm^{-3} [expression (11), below]; and $L=5.2\times10^{17}$ cm which is the path length in Fig. 4 at 0'.8 from the star, over scattering angles 20–70°. It follows that the optical depth $\tau=0.14$ (±0.06 p.e.) at $1/\lambda=1.82$. With the efficiency factors at the other wavelengths it is found that $\tau=0.08$ at $1/\lambda=1.20$, and 0.23 at $1/\lambda=2.78$.

At the August 1965 Conference (Greenberg 1967) a lively discussion occurred on this topic of the optical depth of NGC 7023. Van Houten (1961), for instance, derived an optical depth of 2, but this figure arose from his assumption that HD 200775 is reddened only by the local nebulosity and not at all between the nebula and the earth. This was a poor assumption since the nebula has a radius of only one or two parsecs, but is distant by 290 pc of interstellar space, in which an appreciable amount of the observed extinction must occur. The extinction on the way has been taken into account in this paper by considering *differential* magnitudes of the

TABLE XII. Relative fluxes at various scattering angles in NGC 7023.

Scattering angle interval	$\langle i_1+i_2\rangle$ homog.	coated	Average distance[a] $\times10^{-17}$ cm	Flux per particle $\times10^{46}$	Volume $\times10^{-48}$ cm³	Product[b]
20– 30°	3.173	4.788	4.95	7.76	4.047	3140
30– 40	2.642	3.481	3.66	10.32	2.154	2223
40– 50	2.078	2.285	2.96	10.36	1.406	1457
50– 60	1.551	1.366	2.56	8.28	1.043	864
60– 70	1.104	0.757	2.31	5.63	0.851	479
70– 80	0.756	0.406	2.16	3.46	0.748	259
80– 90	0.503	0.227	2.10	2.04	0.703	143
90–100	0.329	0.146	2.10	1.31	0.703	92
100–110	0.217	0.106	2.16	0.90	0.748	67
110–120	0.148	0.099	2.31	0.74	0.851	63
120–130	0.108	0.097	2.56	0.59	1.043	62
130–140	0.088	0.100	2.96	0.45	1.406	63
140–150	0.080	0.107	3.66	0.32	2.154	69
150–160	0.079	0.113	4.95	0.18	4.047	73

[a] From HD 200775.
[b] Of flux per particle and volume.

TABLE XIII. Grain characteristics.[a]

Grain specifications	$1/\lambda$	$\langle\cos\theta\rangle$	Q_{ext}	Q_{sca}	Q_{pr}	Albedo
$m=1.33-0.15i$	1.06	+0.23	0.496	0.102	0.473	0.206
	1.59	.56	0.894	0.301	0.725	.337
$2a=0.30$	3.18	.90	2.034	1.047	1.092	.515
$m=1.33-0.30i$	1.06	.24	0.866	0.142	0.832	.164
	1.59	.57	1.344	0.364	1.137	.271
$2a=0.30$	3.18	.90	2.202	0.925	1.370	.420
$m=1.57-0.15i$	1.06	.26	0.670	0.269	0.600	.401
	1.59	.57	1.519	0.816	1.054	.537
$2a=0.30$	3.18	.88	3.188	2.031	1.401	.637
	1.20	.34	0.82	0.18	0.76	.22
Mixture *h*	1.82	.63	1.25	0.43	0.98	.34
	2.78	+0.84	1.91	0.83	1.21	0.43
$m_c=1.63-0.82i$	1.11	+0.12	0.122	0.044	0.117	0.361
$m_s=1.33$	1.43	.21	0.221	0.109	0.198	.493
$2a_c=0.08$; $2a_s=0.224$	2.00	.43	0.472	0.295	0.345	.625
	3.33	.74	1.246	0.965	0.532	.774
$m_c=1.40-1.40i$	1.11	.48	0.752	0.253	0.631	.336
$m_s=1.33-0.13i$	1.43	.71	1.090	0.444	0.775	.407
$2a_c=0.02$; $2a_s=0.40$	2.00	.85	1.670	0.841	0.955	.504
	3.33	.96	2.565	1.479	1.145	.577
	1.20	.33	0.50	0.18	0.44	.36
Average, mixture *d*	1.82	.60	0.92	0.47	0.64	.51
	2.78	+0.83	1.60	0.95	0.81	0.59

[a] Forward directivity, $\langle\cos\theta\rangle$; efficiency factors for extinction Q_{ext} scattering Q_{sca}, and radiation pressure Q_{pr}; and the albedo, Q_{sca}/Q_{ext}.

nebula with respect to the illuminating star. Almost all of the polarization is caused at the various scattering angles within the NGC 7023 nebula and all those angles were considered in Sec. IV. On the way the scattering angle is 0°, and only "interstellar type" polarization may be added. [Actually, therefore, the interstellar polarization of the central star should have been subtracted from that of the regions before application of the Mie theory. The observed interstellar polarization (bottom lines, Table II) is, however, relatively small.] A correction for self-extinction within the nebula is taken into account as follows.

The density and polarimetry conclusions are little affected by transmission losses. The distance r [of expression (1)] has been taken into account, as well as the interstellar extinction. The distance R [of expression (9)] has been taken into account by using expression (2). A small correction remains to be made for the extinction over the distance R; this is done with a factor $e^{-\tau R/L}$. The correction factor is 0.88 at scattering angle 25°, 0.90 (35°), 0.92 (45°), 0.93 (55°), and 0.94 (65°). The effect on the polarimetry conclusions, determined by the internal difference of these factors, is negligible. The corrected space density is

$$N=3.8(\pm 1.5 \text{ p.e.})\times 10^{-10} \text{ cm}^{-3}. \quad (11)$$

The effects of multiple scattering should also be considered. From the tables of Coulson, Dave, and Sekera (1960), taking the straight average at scattering angles of 23°, 36°, and 53° with a zenith angle of 180° at the bottom of an atmosphere with zero ground albedo, we have the following polarizations: 27% at $\tau=0.02$, 23% at $\tau=0.2$ and 21% at $\tau=0.4$. At as much as $\tau=0.7$ the polarization has declined to 20% for a total decrease of only 7%. The effects of multiple scattering do not appear to be drastic. However, these numbers are for molecular scattering and they serve only as an illustration.

Multiple scattering cannot affect the density estimates of Sec. VI, at least in a first approximation, since the light that was scattered *into* the pencil beam defined by the focal-plane diaphragm of the telescope equals that scattered *out*.

8. *Grain Characteristics*

Table XIII gives the forward directivity, or asymmetry parameter, evaluated with

$$\langle\cos\theta\rangle=\Sigma[(i_1+i_2)_\theta\cos\theta]/\Sigma(i_1+i_2)_\theta. \quad (12)$$

The summations are made from the Herman–Browning program (Sec. III) over scattering angles $\theta=0$, 37, 53, 66, 78, 90, 102, 114, 127, 143, and 180°. Two mixtures are chosen because they exactly reproduce Fig. 1; other mixtures are, of course, possible. "Mixture *h*" is for *h*omogeneous particles; it is the average of $m=1.33-0.15i$ and $1.33-0.30i$. "Mixture *d*" is the average of the two *d*ouble-composition cases in Table XIII. For each mixture, straight averages are taken of $\langle\cos\theta\rangle$, Q_{ext}, and Q_{sca}; they are graphically interpolated for $1/\lambda=1.20$, 1.82, and 2.78. Q_{pr} is computed as described below, and the albedo is Q_{sca}/Q_{ext}. The other subscripts in Table XIII are *c* for *c*ore and *s* for outer *s*hell.

The radiation pressure is given (van de Hulst 1957, p. 13) by $\pi a^2\rho I_0 Q_{pr}c^{-1}$, where a is the radius, ρ is material density of the particle, I_0 is the intensity of the incident light, and c is the velocity of light. $Q_{pr}=Q_{ext}-\langle\cos\theta\rangle Q_{sca}$ is expressed in terms of the efficiency factors respectively for radiation pressure, for total attenuation, and for scattering; θ is the scattering angle.

In a dynamically steady state of the grain with respect to the illuminating star, the radiation pressure is balanced by gravitation. It is readily shown that the particles in such balance must have

$$a\rho=5.9\times 10^{-5}Q_{pr}(M/M_0)^{2\cdot 3} \quad \text{g cm}^{-2}, \quad (13)$$

where M is the mass of the star and M_0 that of the sun. In the derivation of this "balance condition," the stellar mass–luminosity law is used; torques on the particle and self-extinction within the nebula are neglected. The grains of Table XIII will be pushed outward from a B star if $2a<100\,\mu$, and from a main-sequence G star if $2a<0.5\,\mu$. For purely graphite grains the diameters are $3\,\mu$ and $0.02\,\mu$, respectively. These numbers are for illustration only as more complicated effects enter in.

Around the illuminating star of a reflection nebula, the radiation pressure may have removed the grains from the immediate surroundings. In Fig. 4 at the place of scattering angles 70–110° there are no scatterers. The grains at angles 120–180° do not contribute an appreciable amount of light. This could explain why

the three reflection nebulae observed by Elvius and Hall appear to have the star behind the nebula.

A tentative hypothesis for the evolution of the interstellar grains is summarized as follows.

(a) Late-type stars form absorptive grains (Wickramasinghe 1963; Whitney 1965). The peculiar intrinsic polarizations and polarization dispersions of μ Cephei, V Canum Venaticorum, etc. might be explained with such grains. Radiation pressure eventually moves the smaller ones of these grains out into the interstellar medium.

(b) Accretion in interstellar space (Oort and van de Hulst 1946) forms a dielectric shell around the condensation nucleus.

(c) Radiation pressure sustains the encounters of grains (as well as the high velocities of interstellar clouds and further compression of the clouds into globules, which in turn may play a role in the formation of new stars). The particle encounters, plus, perhaps, evaporation of molecules from the particle skin, cause the upper limitation of sizes of the Oort–van de Hulst distribution. Local conditions can vary such that small variations of the grain characteristics are observed (for instance in Orion; Coyne and Gehrels 1965).

Because of the sharp cutoff in the actual size distribution and because the scattering efficiency is greatest for the largest grains, the *apparent* size distribution is narrow. The wavelength dependence of interstellar polarization and of that of reflection nebulae are, therefore, well defined.

REFERENCES

Blaauw, A. 1963, *Basic Astronomical Data*, K. Aa. Strand, Ed. (The University of Chicago Press, Chicago), p. 401.

Coulson, K. L., Dave, J. V., and Sekera, Z. 1960, *Tables Related to Radiation Emerging from a Planetary Atmosphere with Rayleigh Scattering* (University of California Press, Berkeley and Los Angeles).

Coyne, G. V., and Gehrels, T. 1966, *Astron. J.* **71**, 355 (Paper VIII).

Elvius, A., and Hall, J. S. 1966, *Lowell Obs. Bull.* **135**; also in Greenberg (1967).

Gehrels, T. 1960a, *Astron. J.* **65**, 470 (Paper II).

——. 1960b, *Lowell Obs. Bull.* **4**, 330.

Gehrels, T., and Teska, T. M. 1960, *Publ. Astron. Soc. Pacific* **72**, 115.

Greenberg, J. M., Ed. 1967, *Proceedings of the IAU Colloquium on Interstellar Grains* (National Aeronautics and Space Administration, Washington, D. C.).

Greenstein, J. L., and Aller, L. H. 1947, *Publ. Astron. Soc. Pacific* **59**, 139.

Herman, B. M., and Battan, L. J. 1963, *Electromagnetic Scattering*, M. Kerker, Ed. (Pergamon Press, New York), p. 251.

Houten, C. J., van 1961, *Bull. Astron. Inst. Neth.* **16**, 1.

Hubble, E. 1922, *Astrophys. J.* **56**, 400.

Hulst, H. C., van de 1957, *Light Scattering by Small Particles* (John Wiley & Sons, Inc., New York).

Johnson, H. L. 1965, *Astrophys. J.* **141**, 923.

Johnson, H. L., and Borgman, J. 1963, *Bull. Astron. Inst. Neth.*, **17**, 115.

Keenan, P. C. 1936, *Astrophys. J.* **84**, 601.

LaMer, V. K. 1943, Rept. No. 1857 (Office of Scientific Research and Development, Washington, D. C.); also *Applied Mathematics Series*, No. 4 (National Bureau of Standards, Washington, D. C., 1949).

Lundmark, K. 1922, *Publ. Astron. Soc. Pacific* **34**, 40.

Martel, M.-T. 1958, *Publs. de l'Obs. de Haute-Provence* **4**, No. 20.

Mendoza, E. E. 1958, *Astrophys. J.* **128**, 212.

Oort, J. H., and Hulst, H. C., van de 1946, *Bull. Astron. Inst. Neth.* **10**, 187.

Powell, R. S., Circle, R. R., Vogel, D. C., Woodson, P. D., and Donn, B. 1966, *Melpar Techn. Pre-Print Series* (Melpar Inc., Falls Church, Virginia).

Roark, T. P. 1966, thesis, Rensselaer Polytechnic Institute, Troy, New York.

Stebbins, J., Huffer, C. M., and Whitford, A. E. 1940, *Astrophys. J.* **91**, 20.

Vanýsek, V., and Svatoš, J. 1964, *Acta Univ. Carolinae, Math. Phys.* **1**, 1.

Whitney, C. A. 1965, *Sky and Telescope* **29**, 18.

Wickramasinghe, N. C. 1963, *Monthly Notices Roy. Astron. Soc.* **126**, 99.